

# A comprehensive bifurcation method to analyze the super-harmonic and ultra-harmonic behavior of the acoustically excited bubble oscillator

AJ. SOJAHROOD, D. WEGIERAK, H. HAGHI, R. KARSHAFIAN AND M.C. KOLIOS

Department of Physics, Ryerson University, Toronto, Ontario, Canada  
amin.jafarisojahrood@ryerson.ca

December 3, 2021

## Abstract

*Acoustically excited bubbles are involved in a wide range of phenomena and applications ranging from oceanography to sonoluminescence; they have applications in chemistry, medical imaging, and therapeutic ultrasound. The complexity of bubble dynamics and the limited understanding of their behavior restricts the exploration of their full potential. The bubble oscillator is a highly nonlinear system, which makes it difficult to generate a comprehensive understanding of its oscillatory behavior. One method used to investigate such complex dynamical systems is the bifurcation analysis. Numerous investigations have employed the method of bifurcation diagrams to study the effect of different control parameters on the bubble behavior. These studies, however, focused mainly on investigating the subharmonic (SH) and chaotic oscillations of the bubbles. Super-harmonic (SuH) and ultra-harmonic (UH) bubble oscillations remain under-investigated. One reason is that the conventional method used for generating bifurcation diagrams cannot reliably identify features that are responsible for the identification of SuH and UH oscillations. Additionally, the conventional method cannot distinguish between the UHs and SHs. We introduce a simple procedure for the generation of bifurcation diagrams to address this shortcoming. This method selects the maxima of the bubble oscillatory response and plots them alongside the traditional bifurcation points for the corresponding control parameter. Through applying this method, the oscillatory behavior of the bubble oscillator is analyzed, and stable SuH and UH bubble oscillations are investigated. Based on this new analysis, the conditions for the generation and amplification of UH and SuH regimes are discussed.*

## I. INTRODUCTION

The acoustic bubble [1–12] oscillator is present in many physical phenomena and applications. Bubbles are involved in physical phenomena associated with underwater acoustics and oceanography [2, 12]. Bubbles are used as catalysts for chemical reactions in sonochemistry [13–16] and several non-chemical cleaning applications [17]. Bubble oscillations drive sonoluminescence [15], and are the basis of several medical applications including, but not limited to, blood vessel imaging and treatment monitoring [18, 19], drug delivery [20], blood brain barrier opening [21], high intensity focused ultrasound [22], shock wave lithotripsy [23] and histotripsy and clot lysis [24].

The bubble oscillator is a highly nonlinear dynamical system [1–12, 25–41]; the oscillatory bubble behavior has been referred to as chaotic and complex [1–12, 25–41]. Due to the complex behavior, a comprehensive understanding of the phenomena associated with bubble dynamics is difficult. Consequently, the optimization of applications is a challenging task. Moreover, due

to the incomplete knowledge on the nonlinear behavior of bubbles, many applications are not optimized and this limits progress in the associated fields (e.g., enhanced drug delivery [20]).

Methods of nonlinear dynamics (e.g. resonance curves and bifurcation diagrams) have been extensively applied to investigate bubble behavior [1–7, 25–41]. It has been shown that the bubble oscillator can exhibit  $\frac{1}{2}, \frac{1}{3}, \frac{1}{4}, \frac{1}{5}$  or higher order SHs, as well as period doubling route to chaos [1–7, 25–41]. These studies have shed light on the nonlinear dynamics and bifurcation structure of the bubbles; however, the approaches used in these publications have provided insights primarily on SH and chaotic bubble oscillations. Details of the super-harmonic (SuH) and ultra-harmonic (UH) oscillations remain poorly understood. One of the reasons is that the conventional analysis method only extracts the data after every period of acoustic driving pressure [1,5]. Analysis methods need to be developed to identify and explore SuH and UH oscillations alongside the SH and chaotic regimes.

In this work, we introduce a more comprehensive and simple method to study the SuH and UH bubble oscillations. The bifurcation structure of the bubble oscillator is constructed by plotting the maxima of the stable oscillations of the bubble; which is plotted alongside the conventional bifurcation diagram. Using this method we were able to straightforwardly identify the SuH and UH oscillations and explore the conditions that are required to generate and amplify the SuH and UH oscillations.

This method establishes a framework that provides a more comprehensive understanding of the rich nonlinear behavior of bubbles; consequently, it may help in optimizing current applications and/or can be used to discover new nonlinear bubble behaviors that may result in new applications.

## II. METHODS

### i. The Bubble model

The radial oscillations of the bubbles are numerically simulated by solving the well known Keller-Miksis equation [42]:

$$\rho \left(1 - \frac{\dot{R}}{c}\right) R\ddot{R} + \frac{3}{2}\rho\dot{R}^2 \left(1 - \frac{\dot{R}}{3c}\right) = \left(1 + \frac{\dot{R}}{c} + \frac{R}{c} \frac{d}{dt}\right) \left( (p_0 + \frac{2\sigma}{R_0}) \left(\frac{R_0}{R}\right)^{3k} - \frac{2\sigma}{R} - \frac{4\mu\dot{R}}{R} - P_0 + P_A \sin(2\pi ft) \right) \quad (1)$$

In this equation,  $R$  is radius at time  $t$ ,  $R_0$  is the initial bubble radius,  $\rho$  is the liquid density,  $c$  is the sound speed,  $p_0$  is the atmospheric pressure,  $\sigma$  is the surface tension,  $\mu$  is the liquid viscosity,  $P_A$  and  $f$  are the amplitude and frequency of the applied acoustic pressure.

Oscillations of a bubble generates a backscattered pressure ( $P_{Sc}$ ) which can be calculated by [43]:

$$P_{Sc} = \rho \left(\frac{R}{d}\right) (R\ddot{R} + 2\dot{R}^2) \quad (2)$$

where  $d$  is the distance from the center of the bubble (and for simplicity is considered as 1m in this paper) [43].

Equation 1 is solved using the 4<sup>th</sup> order Runge-Kutta technique; the control parameters of interest are  $R_0$ ,  $f$  and  $P_A$ . The resulting radial bubble oscillations are visualized using the bifurcations diagrams. Bifurcation diagrams of the normalized bubble oscillations  $\frac{R}{R_0}$  are presented as a function of driving pressure. Detailed analysis is presented at select control parameters using

a) the radius versus time curves, b) phase portrait analysis and c) the frequency spectrum of the backscattered pressure.

## ii. Bifurcation diagrams

For highly nonlinear systems like bubble oscillators, small changes in the initial conditions of the system or control parameters can result in large changes in the behavior of the system. However, many studies focus on analyzing the dynamics of the bubbles over discrete values of the control parameters. Due to the complexity and sensitivity of the bubble dynamics to the exposure parameters and initial conditions, the limited values of control parameters used in these studies do not provide a comprehensive understanding of the bubble dynamics. In addition, due to the discrete nature of the investigated parameters, many exposure parameter combinations have not been investigated. Bifurcation diagrams are valuable tools to analyze the dynamics of nonlinear systems where the qualitative and quantitative changes of the dynamics of the system can be investigated effectively over a wide range of the control parameters.

### ii.1 Conventional bifurcation analysis

When dealing with systems responding to a driving force, to generate the points in the bifurcation diagrams vs. the control parameter, one option is to sample from a specific point in each driving period. The approach can be summarized in:

$$Q \equiv (R(\Theta))\{(R(t), \dot{R}(t)) : \Theta = \frac{n}{f}\} \quad \text{where} \quad n = 100, 101 \dots 150 \quad (3)$$

Where  $Q$  denotes the points in the bifurcation diagram,  $R$  and  $\dot{R}$  are the time dependent radius and wall velocity of the bubble at a given set of control parameters of  $(R_0, P_0, P_A, c, k, \mu, \sigma, f)$  and  $\Theta$  is given by  $\frac{n}{f}$ . Points on the bifurcation diagram are constructed by plotting the solution of  $R(t)$  at time points that are multiples of the driving acoustic period. The results are plotted for  $n = 100 - 150$  to ensure a steady state solution has been reached.

### ii.2 Method of peaks

As a more general method, bifurcation points can be constructed by setting one of the phase space coordinates to zero:

$$Q \equiv \max(R)\{(R, \dot{R}) : \dot{R} = 0\} \quad (4)$$

In this method, the steady state solution of the radial oscillations for each control parameter is considered. The maxima of the radial peaks ( $\dot{R} = 0$ ) are identified (determined within 100-150 cycles of the stable oscillations) and are plotted versus the given control parameter in the bifurcation diagrams.

The bifurcation diagrams of the normalized bubble oscillations ( $\frac{R}{R_0}$ ) are calculated using both methods a) and b). When the two results are plotted alongside each other, it is easier to uncover more important details about the SuH and UH oscillations, as well as the SH and chaotic oscillations.

## III. RESULTS

We have considered a bubble with initial diameter of 4 microns. The linear resonance frequency ( $f_r$ ) of the bubble is  $\sim 2.04$  MHz. We have studied the bifurcation structure of the bubble in the form of  $\frac{R}{R_0}$  as a function of the driving acoustic pressure for  $(0.2f_r < f < 3f_r)$  and  $(1\text{kPa} < P_A < 3\text{MPa})$ . Results are shown in Figure 1. Figure 1a-c shows the bifurcation structure of the bubble versus  $P_A$

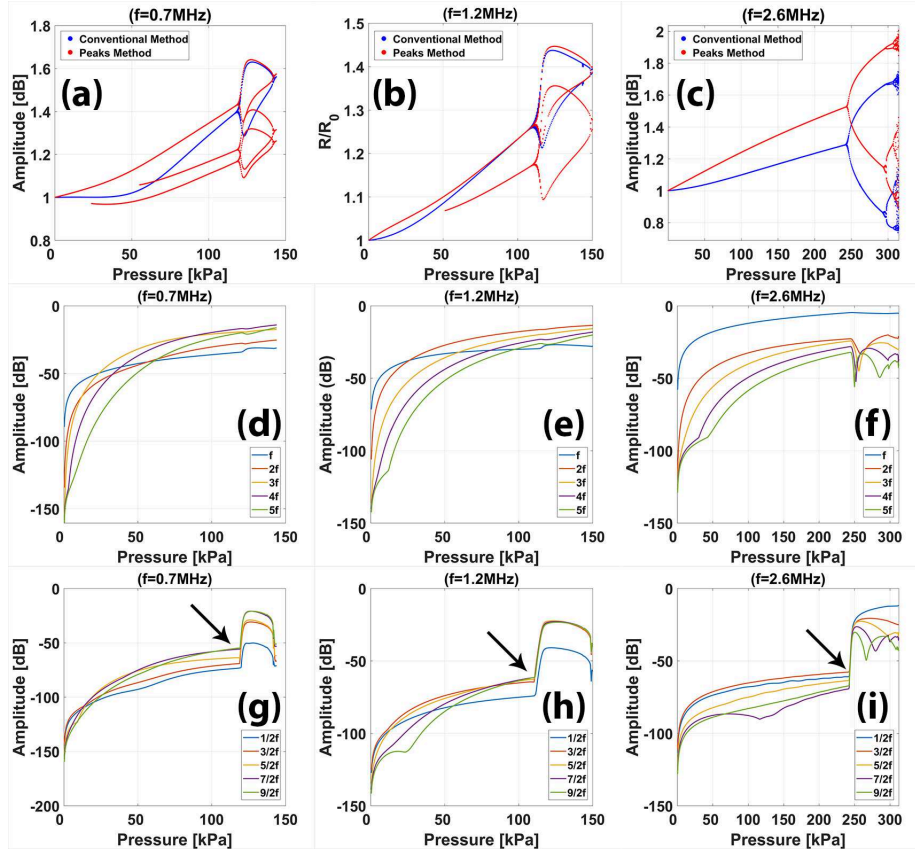


**Figure 1:** Bifurcation structure of the normalized radial oscillations versus acoustic pressure of a 4 micron air bubble immersed in water as constructed by the conventional method (blue) and the peaks method (red): a)  $f=0.7$  MHz, b) 1.2 MHz and c) 2.6 MHz. Harmonics of the backscattered pressure versus acoustic pressure when d)  $f=0.7$  MHz e) 1.2 MHz and f) 2.6 MHz. SH and UH amplitudes of the backscattered pressure versus the acoustic pressure when g)  $f=0.7$  MHz h)  $f=1.2$  MHz i)  $f=2.6$  MHz.

for  $f=0.7$ , 1.2 and 2.6 MHz respectively. To focus on more practical and stable oscillation regimes, we have omitted the parameter ranges that result in chaotic oscillations or bubble destruction ( $\frac{R}{R_0} > 2$  as discussed in detail in [16]). The bifurcation structures that are produced using the conventional method are presented in blue, and the ones produced by the method of peaks are shown in red.

Fig. 1a shows the response of the bubble when  $f=0.7$  MHz. The conventional method reveals a period 1 solution for  $P_A < 118$  kPa and detects the generation of period 2 solution for  $P_A > 120$  kPa. On the other hand, the peaks method reveals the generation of two maxima at  $24 \text{ kPa} < P_A < 56$  kPa and three maxima for  $56 \text{ kPa} < P_A < 118$  kPa. The three maxima undergo period doublings (PDs) resulting in a period 6 solution for  $P_A > 118$  kPa. Examination of the frequency content of the backscattered pressure reveals the underlying phenomenon which results in the discrepancy between the two methods. Figure 1d shows the amplitude of the harmonics and UHs of the backscattered signal. The occurrence of the maxima correlates with the resonance of the harmonic contents of the signal. After a pressure threshold ( $\sim 25$  kPa), the  $3^{rd}$  SuH of the backscattered signal becomes stronger than the fundamental and other SuH harmonics, showing a  $3^{rd}$  SuH resonance. The  $3^{rd}$  SuH saturates for  $P_A > 56$  kPa concomitant with the occurrence of 3 maxima

in the peaks methods. The SH and UH contents of the backscattered signal are shown in Fig. 1g. The simultaneous appearance of period doublings (PDs) in the blue curve and multiple PDs in the red curve are coincident with a sharp increase in the SH and UH content of the backscattered signal (Fig. 1g, arrow); the backscatter at the  $\frac{7}{2}$  (purple) and  $\frac{9}{2}$  UHs (green) are the strongest while the  $\frac{1}{2}$  SH (blue) is the weakest component.

Fig. 1b shows that when sonication frequency is 1.2 MHz the conventional method depicts a similar behavior to  $f=0.7$  MHz (fig. 1a); a linear response is observed for  $P_A < 110$  kPa and radial oscillations undergo a PD for  $P_A > 110$  kPa. The method of peaks reveals a solution with one maximum for  $P_A < 51$  kPa which is similar to the conventional method; above this pressure, however, 2 maxima occur in the bifurcation diagram up until  $P_A = 110$  kPa which are not detected in the conventional method. For  $P_A > 110$  kPa, the oscillations undergo two concomitant PDs resulting in a solution with 4 maxima. The conventional method predicted the same behavior for the two frequencies (0.7 and 1.2 MHz), however, the method of peaks revealed more intricate details of the bubble dynamics. Fig. 1e shows that the second harmonic of the backscattered signal has the strongest amplitude and saturates concomitant with the generation of the initial two maxima at  $\sim 52$  kPa. Fig. 1h illustrates a sharp increase in the amplitude of SH and UHs concomitant with the generation of PDs (arrow) in the blue and red curves as shown in Fig 1b. UH components of the signal are stronger than the SHs ( $\sim 20$  dB) with  $\frac{5}{2}$  and  $\frac{3}{2}$  UHs being the strongest while the  $\frac{1}{2}$  SH is the weakest component.

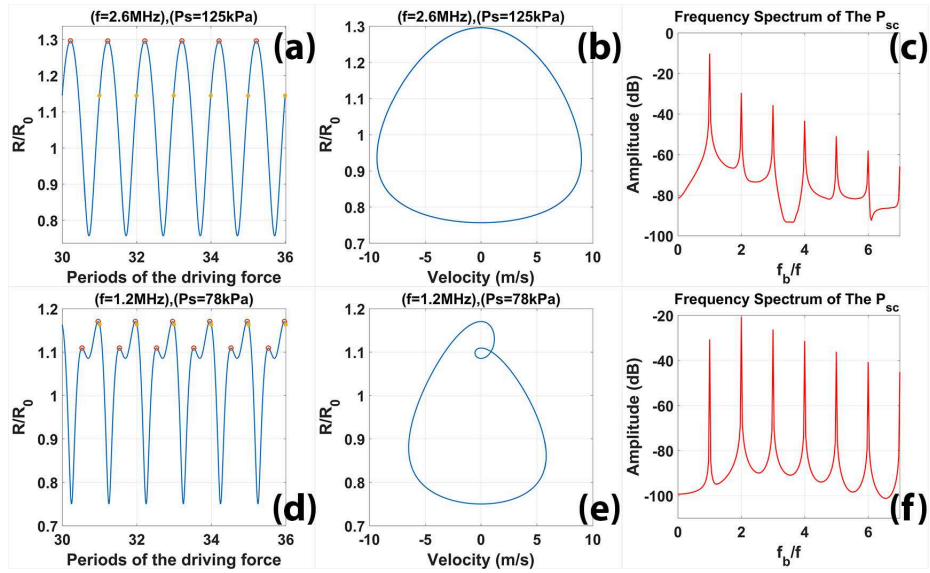
Fig. 1c shows that when  $f=2.6$  MHz the conventional method (blue) and method of peaks (red) depict a similar behavior to  $f=0.7$  MHz and  $f=1.2$  MHz (Fig. 1a, 1b). The oscillations are of period 1 in both graphs until  $P_A=243$  kPa; above this pressure, PD occurs in both methods. The fundamental frequency is the strongest frequency component in the backscattered signal as is shown in Fig. 1f. Figure 1i indicates that the SH and UH components of the signal increase rapidly at pressures at which the PD occurs in Fig. 1c; the SH component is stronger than all the UHs.

To gain a better insight of the oscillation characteristics that the conventional bifurcation analysis method was unable to reveal, a) radial oscillations vs. driving acoustic periods, b) phase portraits and c) backscattered frequency spectra are examined in detail. Exposure parameters were chosen for which both methods give similar predictions and exposure parameters for which the predictions diverged.

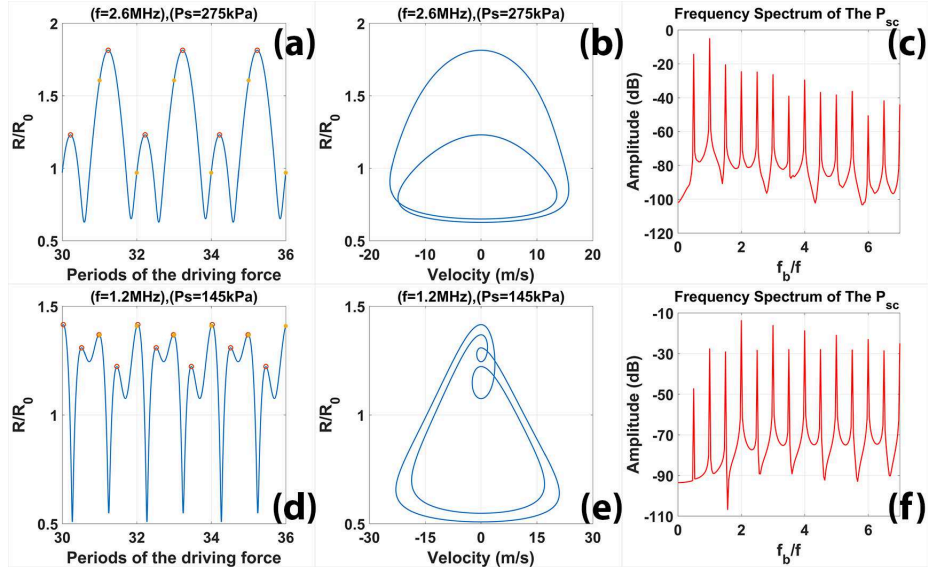
Fig. 2a depicts the radial oscillations of the bubble for  $P_A=125$  kPa and  $f=2.6$  MHz. Inspection of Fig. 1c indicates that a period 1 (P1) oscillation regime is expected. The yellow stars represent the amplitude of radial oscillations after every period, and the red circle illustrates the maxima of the curve. There exists only one value for all red circles and yellow stars; therefore, the signal is a P1 signal with one maximum. The corresponding phase portrait in Fig. 2b is a semi circular orbit, and the fundamental component of the  $P_{Sc}$  is stronger than the SuHs.

Fig. 2d shows the R-T curve that corresponds to  $P_A=78$  kPa and  $f=1.2$  MHz. The signal has two maxima, while the amplitude of the signal at each driving period remains the same. In other words, this suggests a P1 signal with two maxima. Fig. 2e shows that the phase portrait of the bubble undergoes an internal bend; depicting a similar behavior when SHs are present in the curve. However, the absence of SHs are evident in the frequency spectra of the corresponding  $P_{Sc}$  (Fig. 2f) while the  $2^{nd}$  harmonic has the highest value ( $2^{nd}$  harmonic resonance). In this case examination of the maxima provides more complete information about the oscillation characteristics indicating a  $2^{nd}$  SuH resonance.

Figure 3 compares the characteristics of two P2 oscillations; one has two maxima while the other has 4 maxima. Fig 3a shows the R-T curve of the bubble for  $f=2.6$  MHz and  $P_A=275$  kPa. The signal has two maxima (two red dots), and the signal repeats its pattern once every two acoustic driving periods (two yellow stars). The phase portrait (Fig 3b) consists of two circular orbits with one creating another and enclosing it within itself. Fig. 3c depicts the existence of  $\frac{1}{2}$  order



**Figure 2:** Oscillation characteristics of a 4 micron bubble driven at  $f=2.6$  MHz and 125 kPa of pressure: a) Radial oscillations versus driving periods. Yellow dots correspond to  $R(t)$  values at each period (conventional method) and Red dots (peaks method) are positioned at the peaks of the  $R(t)$  curve. b) phase portrait diagrams c) frequency spectrum of the backscattered pressure. Oscillation characteristics of a 4 micron bubble driven with  $f=1.2$  MHz and 78 kPa of pressure: d) Radial oscillations versus driving periods (red shows the peaks and yellow corresponds to  $R(t)$  at each period, e) Phase portrait f) frequency spectrum of the backscattered pressure ( $f_b$  is the frequency of the  $P_{sc}$ ).



**Figure 3:** Oscillation characteristics of a 4 micron bubble driven with  $f=2.6$  MHz and 275 kPa of pressure: a) Radial oscillations versus driving periods (yellow corresponds to  $R(t)$  at each period and red shows the peaks) b) Phase portrait c) frequency spectrum of the backscattered pressure. Oscillation characteristics of a 4 micron bubble driven with  $f=1.2$  MHz and 145 kPa of pressure: d) Radial oscillations versus driving periods (red shows the peaks and yellow corresponds to  $R(t)$  at each period, e) Phase portrait f) frequency spectrum of the backscattered pressure ( $f_b$  is the frequency of the  $P_{sc}$ ).

SH which is stronger than the UH components. Fig. 3d shows the R-T curve of the bubble for  $f=1.2$  MHz and  $P_A=145$  kPa; the signal is of P2 but with 4 distinct maxima. The radial oscillations repeat their pattern once every two acoustic periods (two yellow stars), and each pattern has 4 maxima (4 red dots). The phase portrait has two circular orbits similar to Fig 3b; however, each of these circular orbits underwent an internal bend. The frequency content of the  $P_{sc}$  in Fig. 3f has  $\frac{1}{2}$  order SHs as well as UHs; the  $2^{nd}$  order SuH is the strongest signal, and  $\frac{5}{2}$  and  $\frac{7}{2}$  UHs are stronger than  $\frac{1}{2}$  order SH and other UHs.

#### IV. SUMMARY AND CONCLUSION

We have shown that the conventional method of generating bifurcation diagrams cannot reveal the hidden details of the oscillations that typically result in UH and SuH resonance. We have introduced a simple alternative method to generate the bifurcation diagrams; the method extracts the peaks of the oscillations and plots it as a function of the given control parameter. When this method is applied alongside the conventional method one can reveal hidden details of the bubble oscillations and identify the parameter ranges where SuH, UH or SH oscillations occur. We can briefly categorize the scenarios shown in this paper as follows:

1. The conventional method depicts a P1 oscillation regime, and the maxima method only reveals one maximum. In this case, the oscillation has a P1 resonance and the fundamental frequency component is the strongest in the backscattered signal.  $\frac{1}{2}$  order SH and UHs are generated concomitant with PD in both graphs (constructed by conventional method and method of maxima) and  $\frac{1}{2}$  order SHs, or  $\frac{3}{2}$  UHs are stronger than other UHs.

2. The conventional method depicts a P1 oscillation regime, but maxima method reveals  $n=2,3,\dots$  maxima. In this case, the  $n$ -th order SuH frequency component is the strongest in the backscattered signal. Generation of PD in the conventional method is concomitant with the generation of  $n$ -PDs in the diagram constructed by the peaks method; this correlates with an UH resonance behavior of  $\frac{(2n-1)}{2}$  or  $\frac{(2n+1)}{2}$ ; in other words, these UHs are stronger than the  $\frac{1}{2}$  order SHs and other UHs.
3. The conventional method depicts a P2 oscillation regime, but the maxima method reveals only 1 maximum; in this case, we have a P2 resonance;  $\frac{1}{2}$  order SH frequency component is the stronger than UHs.
4. UH and SHs only exist when the conventional method predicts a P2 oscillations; however, the method of maxima needs to be applied alongside of traditional method to determine whether SH or UH resonance are present, as well as the order of UHs.

The nonlinear behavior of the lipid shell enhances the generation of SHs ( $\frac{1}{2}, \frac{1}{3}, \frac{2}{3}, \frac{1}{4}, \frac{3}{4}, \dots$ ) at very low acoustic pressures and over a more extensive frequency range [45,46]. The behavior of lipid shell MBs are more complex due to the nonlinear response of the encapsulating shell. Implementation of the proposed method in this paper can shine a brighter light on the behavior of lipid coated MBs. Consequently, this approach can be used to optimize the wide range of applications that employ coated MBs. For example, the techniques presented can be used to optimize contrast enhanced techniques employing super harmonics [46, 47] or ultraharmonics [48].

Detailed studies on the effect of initial conditions (ICs) ( $R(0)$  and  $\dot{R}(0)$ ) on the dynamical evolution of the bubble oscillations [28–34] have resulted in the discovery of new nonlinear features [29–34]. For example, depending on the ICs, the bubble has shown to exhibit period 1 (P1), P2 or P3 oscillations [31, 33]. Application of the method proposed in this paper can help to better understand and categorize these nonlinear features, especially in the SuH and UH oscillation regimes. Results using this approach may be used to optimize applications by sending the proper pre-conditioning pulses to manipulate the ICs of the bubble to achieve the desirable behavior.

## REFERENCES

- [1] U. Parlitz, et al., Bifurcation structure of bubble oscillators, *The Journal of the Acoustical Society of America* 88 (1990): 1061-1077.
- [2] A. Prosperetti, L.A. Crum, and K.W. Commander, Nonlinear bubble dynamics, *The Journal of the Acoustical Society of America* 83 (1988): 502-514.
- [3] T.G. Leighton. *The acoustic bubble*. Academic press, 2012.
- [4] W. Lauterborn, and T. Kurz, Physics of bubble oscillations, *Reports on progress in physics* 73 (2010): 106501.
- [5] W. Lauterborn, and U. Parlitz, Methods of chaos physics and their application to acoustics, *The Journal of the Acoustical Society of America* 84 (1988): 1975-1993.
- [6] W. Lauterborn, and E. Cramer, Subharmonic route to chaos observed in acoustics, *Physical Review Letters* 47 (1981): 1445.
- [7] W. Lauterborn, and J. Holzfuss, Acoustic chaos, *International Journal of bifurcation and Chaos* 1 (1991): 13-26.

- [8] A. Prosperetti, and A. Lezzi, Bubble dynamics in a compressible liquid. Part 1. First-order theory, *Journal of Fluid Mechanics* 168 (1986): 457-478.
- [9] L. Hoff, *Acoustic characterization of contrast agents for medical ultrasound imaging*. Springer Science & Business Media, 2001.
- [10] S.M. van der Meer, et al., Microbubble spectroscopy of ultrasound contrast agents, *The Journal of the Acoustical Society of America* 121 (2007): 648-656.
- [11] A. Muthupandian, et al, Bubbles in an acoustic field: an overview, *Ultrasonics Sonochemistry* 14 (2007): 470-475.
- [12] T. G. Leighton, From seas to surgeries, from babbling brooks to baby scans: The acoustics of gas bubbles in liquids, *International Journal of Modern Physics B* 18.25 (2004): 3267-3314.
- [13] K.S. Suslick, *Sonochemistry, science* 247 (1990): 1439-1445.
- [14] B.D. Storey, and A.J. Szeri, Water vapour, sonoluminescence and sonochemistry, *Proceedings of the Royal Society of London A: Mathematical, Physical and Engineering Sciences*. Vol. 456. No. 1999. The Royal Society, 2000.
- [15] L. Crum et al., eds. *Sonochemistry and sonoluminescence*. Vol. 524. Springer Science & Business Media, 2013.
- [16] K. Yasui, et al., Theoretical study of single-bubble sonochemistry, *The Journal of chemical physics* 122 (2005): 224706.
- [17] H. Lais, et al., Numerical modelling of acoustic pressure fields to optimize the ultrasonic cleaning technique for cylinders, *Ultrasonics sonochemistry* 45 (2018): 7-16.
- [18] T. Segers et al., Monodisperse Versus Polydisperse Ultrasound Contrast Agents: Non-Linear Response, Sensitivity, and Deep Tissue Imaging Potential, *Ultrasound in medicine & biology* 44 (2018): 1482-1492.
- [19] K.J. Haworth, et al., Passive imaging with pulsed ultrasound insonations, *The Journal of the Acoustical Society of America*, 132(1) (2012): 544-553.
- [20] K. Ferrara, R. Pollard, and M. Borden, Ultrasound microbubble contrast agents: fundamentals and application to gene and drug delivery, *Annu. Rev. Biomed. Eng.* 9 (2007): 415-447.
- [21] M.A. O'Reilly, et al, Focused-ultrasound disruption of the blood-brain barrier using closely-timed short pulses: influence of sonication parameters and injection rate, *Ultrasound in medicine & biology* 37 (2011): 587-594.
- [22] R. G. Holt, and R.A. Roy, Measurements of bubble-enhanced heating from focused, MHz-frequency ultrasound in a tissue-mimicking material, *Ultrasound in medicine & biology* 27 (2001): 1399-1412.
- [23] S. Yoshizawa, et al., High intensity focused ultrasound lithotripsy with cavitating microbubbles, *Medical & biological engineering & computing* 47 (2009): 851-860.
- [24] K.B. Bader., K.J. Haworth, H. Shekhar, A.D. Maxwell, T. Peng, D.D. McPherson, and C.K. Holland, Efficacy of histotripsy combined with rt-PA in vitro. *Physics in Medicine & Biology* 61, (2016): 5253.
- [25] A.J. Sojahrood and M.C. Kolios, Classification of the nonlinear dynamics and bifurcation structure of ultrasound contrast agents excited at higher multiples of their resonance frequency, *Physics Letters A* 376 (2012): 2222-2229.

- [26] S. Behnia, A.J. Sojahrood, W. Soltanpoor and O. Jahanbakhsh, Suppressing chaotic oscillations of a spherical cavitation bubble through applying a periodic perturbation, *Ultrasonics sonochemistry* 16 (2009): 502-511.
- [27] A.J. Sojahrood et al., Influence of the pressure-dependent resonance frequency on the bifurcation structure and backscattered pressure of ultrasound contrast agents: a numerical investigation, *Nonlinear Dynamics* 80 (2015): 889-904.
- [28] S. Behnia, A.J. Sojahrood, W. Soltanpoor, and L. Sarkhosh, Towards classification of the bifurcation structure of a spherical cavitation bubble, *Ultrasonics* 49(8) (2009): 605-610.
- [29] F. Hegedűs, and L. Kullmann, Basins of attraction in a harmonically excited spherical bubble model, *Periodica Polytechnica Mechanical Engineering* 56 (2012): 125-132.
- [30] F. Hegedűs, et al, Non-feedback technique to directly control multistability in nonlinear oscillators by dual-frequency driving, *Nonlinear Dynamics* (2018): 1-21.
- [31] F. Hegedűs, and C. Kalmár, Dynamic stabilization of an asymmetric nonlinear bubble oscillator, *Nonlinear Dynamics*: 1-18.
- [32] F. Hegedűs, Topological analysis of the periodic structures in a harmonically driven bubble oscillator near Blake's critical threshold: Infinite sequence of two-sided Farey ordering trees, *Physics Letters A* 380-10 (2016): 1012-1022.
- [33] R.Varga, and F. Hegedűs, Classification of the bifurcation structure of a periodically driven gas bubble, *Nonlinear Dynamics* 86 (2016): 1239-1248.
- [34] F. Hegedűs, C. Hős, and L. Kullmann, Stable period 1, 2 and 3 structures of the harmonically excited Rayleigh–Plesset equation applying low ambient pressure, *The IMA Journal of Applied Mathematics* 78 (2012): 1179-1195.
- [35] Y. Zhang, Chaotic oscillations of gas bubbles under dual-frequency acoustic excitation, *Ultrasonics sonochemistry* 40 (2018): 151-157.
- [36] Y. Zhang, G. Yuhang, and D. Xiaoze, Stability mechanisms of oscillating vapor bubbles in acoustic fields, *Ultrasonics sonochemistry* 40 (2018): 808-814.
- [37] Y. Zhang, and S. Li. Bubble dynamics under acoustic excitation with multiple frequencies, *IOP Conference Series: Materials Science and Engineering*. Vol. 72. No. 1. IOP Publishing, 2015.
- [38] Y. Zhang, and S. Shengcai, Combination and simultaneous resonances of gas bubbles oscillating in liquids under dual-frequency acoustic excitation, *Ultrasonics sonochemistry* 35 (2017): 431-439.
- [39] S.A. Suslov, A.Ooi, and R. Manasseh, Nonlinear dynamic behavior of microscopic bubbles near a rigid wall, *Physical Review E* 85 (2012): 066309
- [40] F. Dzaharudin , A. Ooi, & R. Manasseh, Effects of boundary proximity on monodispersed microbubbles in ultrasonic fields. *Journal of Sound and Vibration* 410, (2017): 330-343
- [41] F. Dzaharudin , S.A. Suslov, R. Manasseh and A. Ooi, Effects of coupling, bubble size, and spatial arrangement on chaotic dynamics of microbubble cluster in ultrasonic fields, *The Journal of the Acoustical Society of America* 134 (2013): 3425-3434.
- [42] J.B. Keller, and M. Miksis, Bubble oscillations of large amplitude, *The Journal of the Acoustical Society of America* 68 (1980): 628-633.

- [43] S. Hilgenfeldt, D. Lohse, and M. Zomack, Sound scattering and localized heat deposition of pulse-driven microbubbles, *The Journal of the Acoustical Society of America* 107 (2000): 3530-3539.
- [44] A.J Sojahrood R. Karshafian, and M.C. Kolios, Bifurcation structure of the ultrasonically excited microbubbles undergoing buckling and rupture, *Proceedings of Meetings on Acoustics ICA2013*. Vol. 19. No. 1. ASA, 2013.
- [45] A.J Sojahrood R. Karshafian, and M.C. Kolios, Detection and characterization of higher order nonlinearities in the oscillations of Definity at higher frequencies and very low acoustic pressures, *Ultrasonics Symposium (IUS), 2012 IEEE International*. IEEE, 2012.
- [46] S.E. Shelton, et al., Molecular acoustic angiography: A new technique for high-resolution superharmonic ultrasound molecular imaging, *Ultrasound in medicine & biology* 42 (2016): 769-781.
- [47] A. Bouakaz, et al., Super harmonic imaging: a new imaging technique for improved contrast detection, *Ultrasound in medicine & biology* 28 (2002): 59-68.
- [48] V. Daeichin, et al., Subharmonic, non-linear fundamental and ultraharmonic imaging of microbubble contrast at high frequencies, *Ultrasound in medicine & biology* 41 (2015): 486-497.